



RESEARCH LETTER

10.1002/2016GL067907

Key Points:

- Coseismic and early postseismic observations of M_w 7.8 Gorkha, Nepal, earthquake are presented
- The postseismic surface uplift and subsidence is found to be opposite to that of coseismic motion
- An afterslip occurred mainly toward downdip and eastward of the coseismic slip asperity

Supporting Information:

- Supporting Information S1

Correspondence to:

P. S. Sunil,
sunilps@iigs.iigm.res.in

Citation:

Sreejith, K. M., P. S. Sunil, R. Agrawal, A. P. Saji, D. S. Ramesh, and A. S. Rajawat (2016), Coseismic and early postseismic deformation due to the 25 April 2015, M_w 7.8 Gorkha, Nepal, earthquake from InSAR and GPS measurements, *Geophys. Res. Lett.*, 43, doi:10.1002/2016GL067907.

Received 22 JAN 2016

Accepted 11 MAR 2016

Accepted article online 18 MAR 2016

Coseismic and early postseismic deformation due to the 25 April 2015, M_w 7.8 Gorkha, Nepal, earthquake from InSAR and GPS measurements

K. M. Sreejith¹, P. S. Sunil², Ritesh Agrawal¹, Ajish P. Saji², D. S. Ramesh², and A. S. Rajawat¹

¹Geosciences Division, Space Applications Center (ISRO), Ahmedabad, India, ²Indian Institute of Geomagnetism (DST), Navi Mumbai, India

Abstract Analysis of Interferometric Synthetic Aperture Radar (InSAR) and Global Positioning System (GPS) data reveals coseismic and early postseismic (4–88 days) surface displacements associated with the 25 April 2015, M_w 7.8 Gorkha, Nepal, earthquake. The pattern of early postseismic surface uplift and subsidence is found to be opposite to that of the coseismic motion. InSAR and GPS data were jointly inverted for coseismic and postseismic slip on the Main Himalayan Thrust (MHT). We consider a complex *ramp-flat-ramp-flat* subsurface structure of the MHT with four connected fault planes dipping toward north from the Main Frontal Thrust (MFT). The inverted coseismic slip distribution follows an elliptical pattern, extending east-southeastward from the hypocenter with maximum amplitude of 5.7 m above the upper edge of the midcrustal ramp. We infer early postseismic afterslip (4–16 days) of 0.2–0.47 m toward downdip of the coseismic slip asperity and another patch with 0.1–0.2 m slip toward east. The shallow portion of the MHT toward south is found to have remained unruptured during the earthquake, nor did it slip aseismically after the earthquake, suggesting possibility of large events in the future.

1. Introduction

The destructive 25 April 2015, Gorkha, Nepal, earthquake of magnitude M_w 7.8 is one of the largest earthquakes (hereafter referred as Gorkha earthquake) to have struck Nepal since the 1934 Nepal-Bihar earthquake of M_w 8.2 [Sapkota *et al.*, 2012]. Moment tensor solution from teleseismic data suggests that the Gorkha earthquake occurred on a 10–20° dipping subhorizontal blind thrust fault at about 15 km depth with a strike of 290° from north [U.S. Geological Survey-National Earthquake Information Center (USGS-NEIC), 2015; *Global Centroid Moment Tensor Catalogue (GCMT)*, 2015]. The largest aftershock occurred on 12 May 2015 about 150 km east of the main shock, ruptured easternmost part of the main fault (Figure 1). The Gorkha earthquake ruptured the Main Himalayan Thrust (MHT), a detachment boundary between the Indian and Eurasian Plates, which absorbs about 20 mm/yr convergence in Nepal [Ader *et al.*, 2012; Bilham, 2015]. The elastic strain energy stored during interseismic period is released periodically due to earthquakes and causing ruptures along locked brittle upper part of the MHT system [Bilham *et al.*, 2001].

After the Gorkha event, the coseismic deformation due to the earthquake was mapped using InSAR and GPS data by different groups [Avouac *et al.*, 2015; Diao *et al.*, 2015; Feng *et al.*, 2015; Galetzka *et al.*, 2015; Lindsey *et al.*, 2015; Wang and Fialko, 2015; Zhang *et al.*, 2015]. Geodetic inversion of these data has provided detailed slip distribution pattern on the causative fault. However, in all these studies, a highly simplified geometry of the causative fault (MHT) with a constant or uniformly varying dip angle was used. In the present study, we invert the coseismic and early postseismic InSAR and GPS data using a more realistic fault model with four-segment fault planes having variable dip angles representing the *ramp-flat-ramp-flat* geometry of the MHT as inferred from seismic, electrical, and geodetic studies [Zhao *et al.*, 1993; Pandey *et al.*, 1995; Lemonnier *et al.*, 1999; Cattin and Avouac, 2000]. Second, for the first time, we map the spatiotemporal evolution of the early postseismic deformation of the Gorkha earthquake using InSAR and GPS data.

2. Data Analysis and Results

We have used SAR data from Sentinel-1 satellite and near-field GPS data from four stations (CHLM, KKN4, NAST, and SNDL) of Nepal Geodetic Network for the coseismic and postseismic investigations of the Gorkha earthquake. Line of Sight (LOS) deformation maps were generated using 11 interferograms

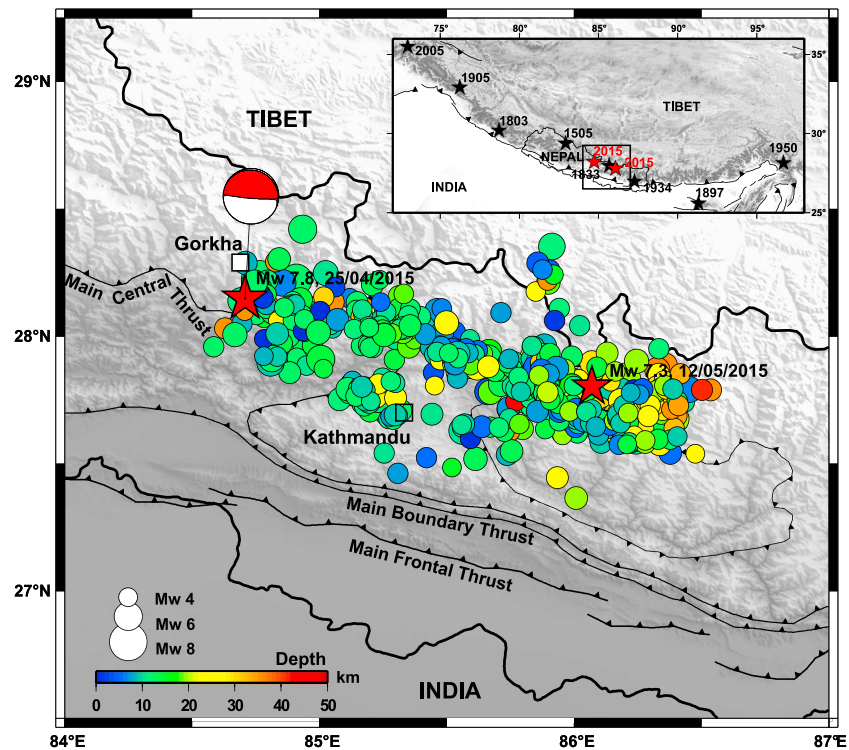


Figure 1. Map showing the epicenter locations of the 25 April 2015 (M_w 7.8) Gorkha earthquake and 12 May 2015 (M_w 7.3) aftershock (red stars) along with other aftershocks [after Adhikari *et al.*, 2015] in circles. Main Frontal Thrust (MFT), Main Boundary Thrust (MBT), and Main Central Thrust faults (MCT) are shown as black lines. The inset map represents the present study area in rectangle with great and large earthquakes since 1505 in stars.

(Table S1 in the supporting information) after correcting for orbital ramps and atmospheric phase delay (Text S1 and Figures S1 and S2). After detailed analysis of coherence, orbital ramp effects, and atmospheric artifacts, we chose coseismic interferogram generated during 17 April 2015 and 29 April 2015 (17/04/2015–29/04/2015) for the analysis. For postseismic deformation analysis the first Sentinel-1 data acquisition after the Gorkha earthquake (29 April 2015) was used as reference date. Deformation maps were generated with respect to this date using acquisitions on 11 May 2015 (29/04/2015–11/05/2015), 4 June 2015 (29/04/2015–04/06/2015), and 22 July 2015 (29/04/2015–22/07/2015), respectively (Table S1). This enables us to map the cumulative temporal and spatial evolution of early postseismic deformation starting from the fourth day after the main shock in three epochs: 4–16 days, 4–40 days, and 4–88 days (Figure 2).

Coseismic and initial 3 months postseismic GPS displacements have been derived from continuous position time series of four stations (Figures 2 and S2). To understand the characteristics postseismic deformation mechanism, logarithmic [Marone *et al.*, 1991] and exponential [Scholz, 1990] model decay fittings were performed. The time series showed better fit with logarithmic than exponential model (Figure S3). The magnitude of the GPS postseismic displacement at available InSAR epochs was estimated from the optimal log coefficients fit to the individual time series.

The deformation map generated from the coseismic interferogram (Figure 2a) suggests an upliftment of about 1 m near Kathmandu and a subsidence of about 0.8 m toward north along the LOS of the pertinent satellite. The near-field GPS station KKN4 within the positive LOS deformation lobe shows horizontal motion in S-SW direction with maximum amplitude of 1.88 m and up to 1.28 m in vertical direction, whereas the GPS station CHML located at the negative LOS deformation lobe shows prominent subsidence of about 0.6 m (Figure 2a).

The most striking feature of the early postseismic deformation is the reversal in the direction of ground motion with respect to the coseismic deformation (Figures 2a–2e). Further, it is observed that the postseismic

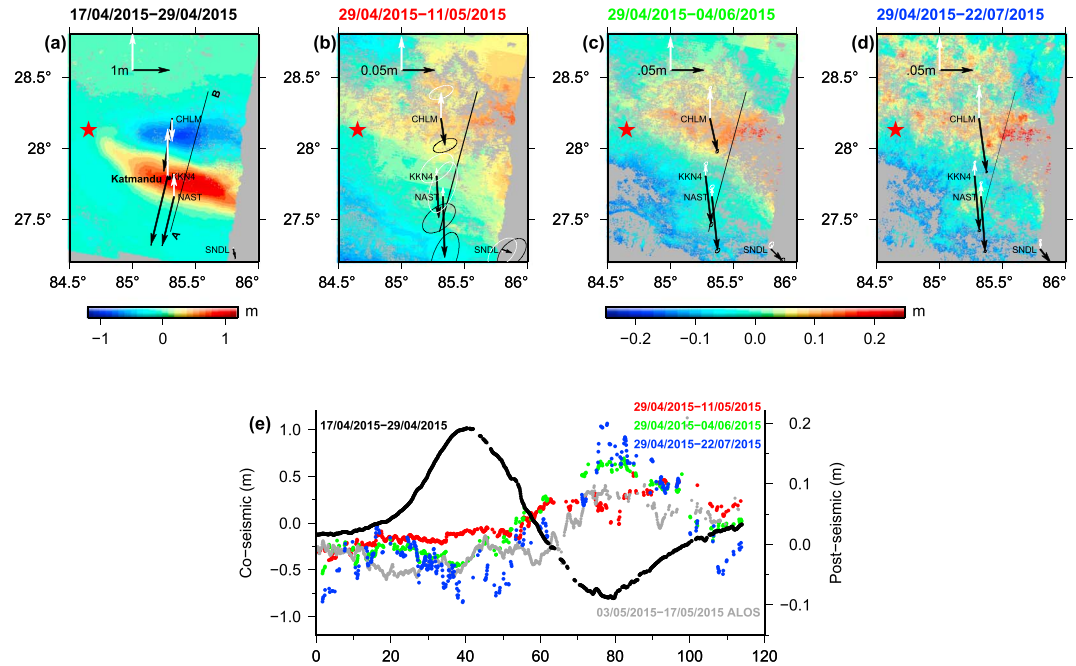


Figure 2. (a) Coseismic and postseismic deformation maps at different epochs (b–d) generated by InSAR analysis. GPS data offsets corresponding to InSAR epochs in horizontal (black arrow) and vertical (white arrow) directions are shown. (e) The profiles of InSAR data during coseismic (left Y axis) and different postseismic epochs (right Y axis) as indicated by respective color codes along the section AB. Postseismic deformation along section AB obtained from ALOS interferogram [Lindsay et al., 2015] is also shown (gray dots).

deformation pattern is broader in wavelength and appears to be asymmetric with upliftment toward north of 0.05–0.15 m (corresponding to the coseismic subsidence) and a subsidence up to 0.07 m toward south (corresponding to the coseismic upliftment) along the LOS (Figures 2b–2e). The InSAR observations are well supported by the postseismic GPS displacements derived for the same epochs. The direction of horizontal GPS vectors changed from south-southwest direction during the coseismic period (Figure 2a) to south-southeast during the postseismic period (Figures 2b–2d). In vertical direction, the GPS station CHLM which showed subsidence during the coseismic period shows prominent upliftment of about 0.06 m during the postseismic period. The complementary nature of coseismic and postseismic deformation, the broader wavelength of later, and the logarithmic fit to the postseismic time series GPS data together indicate afterslip at deeper parts of the causative fault.

3. Slip Models

3.1. Coseismic Slip Model

The structure of the MHT in central Nepal is well established from geophysical studies and consists of a frontal ramp, southern flat, midcrustal ramp, and northern flat segments. For modeling purpose, we approximate the geometry of MHT with four rectangular connected fault segments. Dip angles and widths of the model fault segments were adopted from the integrated seismic and electrical section across the central Nepal [Avouac, 2003]. The first fault segment extends to about 10 km toward north from the MFT with a dip of 30° down to 5 km and represents the frontal ramp. The second segment is relatively flat with a dip = 5°, extends 65 km farther north, and joins 50 km wide third segment which has a deeper dip angle of 16° called the midcrustal ramp. The shallow dipping (6°), 50 km wide fourth segment represents the aseismically creeping portion of the MHT. The strike of the fault segments considered is 292° and has variable rakes (90°–100°). Each of the model fault segments is subdivided into patches with sizes determined by their depth and width to ensure maintaining uniform resolution of slip [Fialko, 2004]. The preferred sizes of the patches range from 2 × 2 km² of the shallow and narrow first fault segment to 10 × 10 km² of the deeper and wider fourth fault segment.

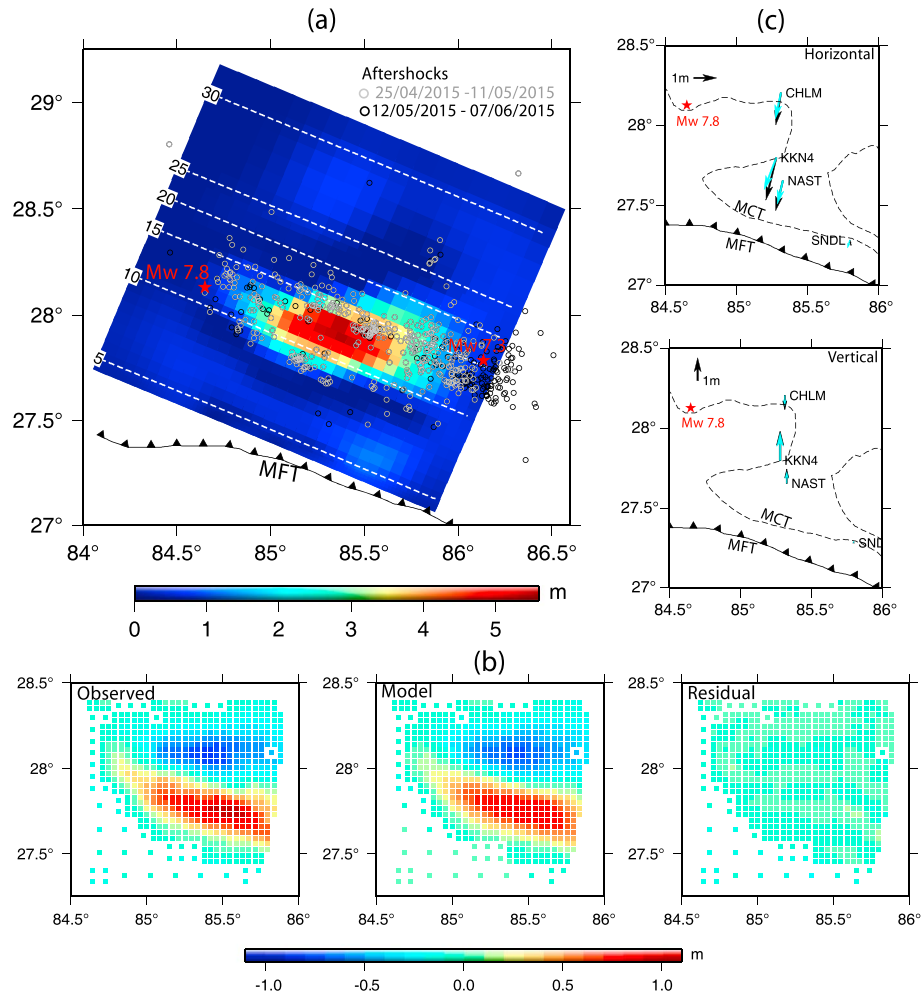


Figure 3. (a) Coseismic slip model of the 25 April 2015 Gorkha earthquake. Depth to the fault (dashed white lines) and aftershocks during 25/04/2015-11/05/2015 (gray dots) and 12/05/2015-07/06/2015 (black circle) are shown. (b) Observed, modeled, and residual coseismic InSAR deformation maps. (c) Observed (black) and modeled (cyan) coseismic GPS deformation vectors.

We inverted coseismic InSAR and GPS data to model the slip on the causative fault of the Gorkha earthquake assuming linear superposition of rectangular dislocations in an elastic half-space [Okada, 1985]. We use SDM (steepest descent method) iterative algorithm [Wang *et al.*, 2013] for the constrained least squares optimization to solve for the dip-slip and strike-slip components. The optimum smoothing factor ($\gamma^2 = 0.2$) for the inversion was chosen from the trade-off curve between the model roughness and misfit (the *L* curve) (Figure S4a). The optimum weighting ratio between InSAR and GPS ($\alpha = W_{\text{InSAR}}/W_{\text{GPS}}$) is chosen as 2 based on the trade-off curve between α and solution misfit (Figure S4b).

The inverted coseismic deformation closely matches with the observed InSAR and GPS deformations (Figure 3). The coseismic rupture of the Gorkha earthquake is dominated by thrust slip with a maximum value of 5.65 m along with a minor component from right-lateral slip (0.6 m) (Figure S6a). The maximum coseismic slip is about 5.7 m at a depth of 12 km (Figure 3a). The total moment released by the earthquake is calculated as 6.95×10^{20} Nm, which corresponds to a magnitude of M_w 7.829, which closely agrees with that obtained from seismic waveform inversion (M_w 7.8) [USGS-NEIC, 2015].

3.2. Early Postseismic Slip Model

The InSAR data pair (29/04/2015-11/05/2015) along with the GPS-derived velocity for a period of 13 days is selected for afterslip inversion as it represents early postseismic movements (4–16 days after the Gorkha earthquake), which are not influenced by M_w 7.3 largest aftershock occurred on the same fault on 12 May

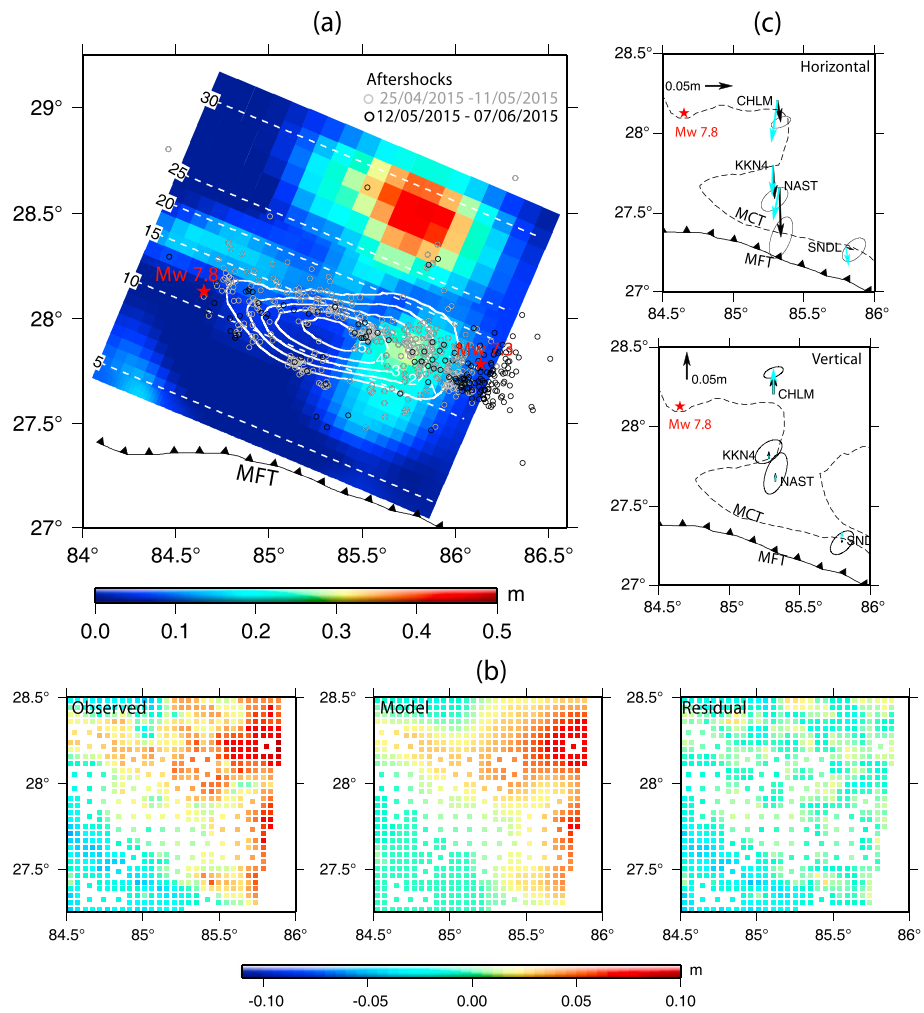


Figure 4. (a) Postseismic slip model for the 25 April 2015 Gorkha earthquake. Depth to the fault (dashed white lines) and aftershocks during 25/04/2015-11/05/2015 (gray dots) and 12/05/2015-07/06/2015 (black circle) are shown. Coseismic slip is shown as white contours (in meters). (b) Observed, modeled, and residual postseismic InSAR deformation maps. (c) Observed (black) and modeled (cyan) postseismic GPS deformation vectors.

2015. The afterslip inversion was carried out using the same fault parameterization as that of the coseismic slip inversion. However, the rake angle was allowed to vary from 90° to 120° in order to account for the post-seismic dextral motion shown in the GPS data. The optimal values for model roughness ($\gamma^2 = 0.175$) and relative weighting factor ($\alpha = 2$) were determined using respective trade-off curves as in the case of coseismic inversion (Figures S5a and S5b). The modeled interferogram could predict major features of the observed data except for a linear patch toward south (Figure 4), which would be probably related with atmospheric disturbances. The postseismic slip has magnitude about 0.2–0.47 m that appears to have predominantly occurred downdip of coseismic slip (Figure 4a). Another patch with less amount of slip (~ 0.1 – 0.2 m) is also found east of the coseismic slip asperity. The postseismic motion has significant contribution from right-lateral slip, particularly along the downdip patch, where the maximum right-lateral slip is about 0.23 m and accounts for about half of the dip-slip component (Figure S6b). The total moment released by the early afterslip is about 1.05×10^{20} Nm corresponding to a moment magnitude of M_w 7.28.

4. Discussions

The coseismic slip due to the Gorkha earthquake was previously estimated using highly simplified planar or curved fault geometry for the MHT. The preferred dip angle of MHT for the earthquake source modeling

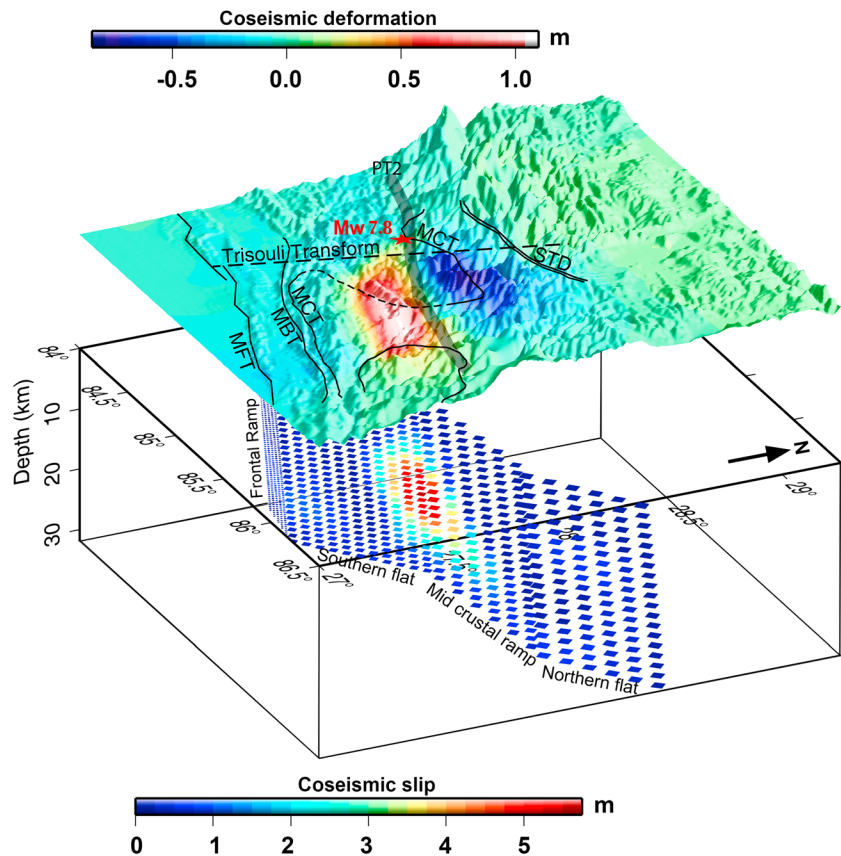


Figure 5. Three-dimensional illustration of the coseismic slip and related surface deformation due to the Gorkha earthquake.

varied from 7° [Wang and Fialko, 2015] to 11° [Lindsey et al., 2015]. Therefore, we have carried out a series of inversions, both coseismic and postseismic, assuming planar as well as curved fault geometry for a range of dip values (5° – 15°). We observed that both planar and curved fault models with shallow dip angles ($<7^\circ$) have lower misfit compared to that of steeper angles dip ($>10^\circ$). Planar and curved fault solutions with a dip angle of 5° closely match with present four-segment model within misfit of $<5\%$. However, we prefer the four-segment fault model over a shallow dipping planar/curved fault models as it provides a better insight to the subsurface slip distribution along the MHT which has implications in modeling long-term strain along the Himalayan collision zone and for earthquake hazard assessment.

4.1. Structural Control on Coseismic Rupture

During the Gorkha event, the MHT is partially ruptured toward east-southeast direction along the dip and strike direction of coseismic slip, which can provide constraints on the geometric control of the earthquake rupture propagation. Our model suggests that the nucleation of the earthquake appears to have initiated at the lower bend portion of the flat midcrustal ramp transition (Figures 3a and 5). The downdip propagation of the rupture along the steep ramp must have been restricted due to sharp changes in frictional and rheological properties along the ramp [Berger et al., 2004]. However, updip rift propagation along the fully locked flat portion of the MHT would have caused breaking of the shallow part of MHT resulting in coseismic surface upliftment near MFT. Conversely, during the Gorkha earthquake surface subsidence occurred about 40–50 km toward north of MFT (Figures 3a and 5). Grandin et al. [2015] suggested that the updip arrest of the rift propagation appears to be unrelated to variation in local coupling ratios and instead could be related to structural complexities along the MHT. It is interesting to note that the positive and negative coseismic InSAR deformation fields are separated by a physiographical boundary (PT2) as identified by Wobus et al. [2005] (Figure 5). Parameswaran et al. [2015] suggested that a component of slip could have emerged through PT2. However, it seems difficult to reconcile such an out-of-sequence thrusting during the Nepal earthquake as (a) no major surface rupture is reported neither from field or satellite observations and (b)

the deformation field across the PT2 does not have a drastic change which clearly rules out the possibility of a shallow slip. However, we speculate that the thrust plane connecting the MHT and PT2 must have acted as a hinge zone that controlled the rupture propagation and slip partitioning along the MHT.

For Great Himalayan Earthquakes, in general, it is believed that the ruptures are controlled by asperities and structural complexities [Feldl and Bilham, 2006; Mugnier *et al.*, 2013]. Grandin *et al.* [2015] suggested that the rupture area of the Gorkha earthquake is confined to a structural asperity, the Kathmandu klippe, between 84.5° and 86°E (Figure 5). Further, we infer that the coseismic surface deformation occurs mainly toward east of a major lateral crustal ramp, the NE-SW trending Trisouli Transfer Zone [Berger *et al.*, 2004] (Figure 5). Backprojection and finite-fault inversion results [Fan and Shearer, 2015; Yagi and Okuwaki, 2015; Denolle *et al.*, 2015] also suggest that this runaway rupture propagation could be related to the Trisouli Transform. On the other hand, the eastward propagation of the rupture terminates abruptly near 86.2° and approximately bonded by the estimated rupture area of the M_w 8.2 1934 Nepal-Bihar earthquake [Sapkota *et al.*, 2012].

4.2. Coseismic and Postseismic Slip Distribution Along MHT

Comparison of coseismic and postseismic slip models clearly suggests that afterslip was triggered mainly toward downdip of the coseismic asperity (Figures 3a and 4a). However, the tiny amount of postseismic slip patch existing toward the east appears to overlap with the coseismic slip asperity (Figure 4a). This could be attributed to the initial stage of stress-driven afterslip that may have occurred prior to the acquisition of the first postseismic SAR data on 29 April 2015. Further, in this time period, the postseismic rupture expansion along the fault plane must have happened mainly toward east, which is also marked by pattern of aftershocks between the days of main shock and 11 May 2015 (Figures 3 and 4). The cluster of aftershocks between farther toward east appears to be associated with the M_w 7.3 largest aftershock event that occurred on 12 May 2015. The coseismic rupture was dominated by thrust motion, whereas the early postseismic afterslip shows right-lateral slip (Figures S6a and S6b). This could be probably associated with the changes in the principal axis of stress field induced by the main shock as observed for the 2011 M_w 7.1 Van (Turkey) earthquake [Feng *et al.*, 2014].

While coseismic slip occurred along the upper part of the midcrustal ramp, majority of the postseismic slip occurred below the lower edge of the midcrustal ramp, where relatively ductile interseismic creeping zone exists (Figure 4b) [Ader *et al.*, 2012]. This clearly indicates that the afterslip is predominantly aseismic in nature. It turns out that the segment of MHT where comparatively steep midcrustal ramp interacts with flat fault segments acted as a barrier for stress buildup in central Nepal Himalaya and seems to spawn earthquakes. This is evident from the steeper rupture planes (10°–20°) reported for several earthquakes in the Himalayan arc [Satyabala and Bilham, 2006]. Elsewhere, Chuang *et al.*, 2013 suggest that the faulting of midcrustal level ramp structure caused the 2013 Nantou earthquake series in Taiwan.

The coseismic and postseismic deformation sequences of the Gorkha earthquake can be compared to those of the 8 October 2005 Pakistan earthquake [Jouanne *et al.*, 2011], where the coseismic slip occurred along the lower edge of the ramp followed by afterslip along the flat region toward north. Similarly, continental earthquakes such as the 1995 Colima-Jalisco earthquake (M_w 8.0) [Hutton *et al.*, 2001] and the 1999 Chi-Chi earthquake (M_w 7.3) [Hsu *et al.*, 2002] were followed by afterslip downdip of the seismic rupture extending to the creeping zone rather than within the locked fault zone.

4.3. Earthquake Potential on MHT

Along the Himalayan arc, the MHT is locked from surface closer to the MFT to over a distance of about 100 to 120 km where the stress tends to considerably accumulate and release interseismic strain energy. Recent geodetic studies suggest that during the interseismic period, aseismic thrust displacement occurs in the deeper and ductile northern part of the MHT alone, while no slow earthquakes have been detected in the brittle, externally locked part of the MHT [Jouanne *et al.*, 2004; Bettinelli *et al.*, 2006; Ader *et al.*, 2012]. The 2015 Gorkha earthquake occurred on a seismic gap between the 1934, 1833, and 1505 events (Figure 1) and ruptured the deeper portion of the MHT toward east-southeast direction. However, the afterslip model in the present study suggests that the postseismic relaxation is confined to the downdip and eastern portions of the coseismic asperity. This indicates that a large stress field induced by the thrust motion toward south during the Gorkha earthquake is not relaxed immediately in the early postseismic period. It increases the risk of another major event as postulated by Bilham [2015]. However, continued geodetic observations are much needed to understand the detailed postseismic behavior of the MHT toward south.

5. Conclusions

Coseismic and early postseismic deformation studies of the Gorkha earthquake using InSAR and GPS data led to the following conclusions.

1. The early postseismic surface uplift and subsidence associated with the M_w 7.8 Gorkha earthquake is found to be opposite in direction to that of the coseismic motion.
2. The GPS time series indicate a logarithmic decay in postseismic velocities signifying that stress-driven afterslip contributes toward the postseismic relaxation mechanism.
3. The coseismic slip distribution follows an elliptical pattern along the rupture plane, extending east-southeastward from the hypocenter with maximum amplitude of 5.7 m along the upper edge of the midcrustal ramp.
4. An early postseismic afterslip (4–16 days) of 0.2–0.47 m surrounding the coseismic slip asperity is inferred, mainly toward downslip and eastward.
5. The shallow portion of the MHT toward south has neither been ruptured during the Gorkha earthquake nor slipped aseismically after the earthquake, suggesting possibility of large events in future.

Acknowledgments

This work was carried out jointly by SAC-ISRO and IIG-DST as a part of the DMSP R&D program. We thank S.K. Arora, two anonymous reviewers, and Editor Andrew Newman for their constructive comments. Rongjiang Wang and Faqi Diao are acknowledged for their help in using SDM code. Tapan Misra, B.S. Gohil, and Raj Kumar from SAC have supported the collaborative studies. Figures were prepared using GMT software (<http://gmt.soest.hawaii.edu/>).

References

- Ader, T., et al. (2012), Convergence rate across the Nepal Himalaya and interseismic coupling on the Main Himalayan Thrust: Implications for seismic hazard, *J. Geophys. Res.*, *117*, B04403, doi:10.1029/2011JB009071.
- Adhikari, L. B., et al. (2015), The aftershock sequence of the 2015 April 25 Gorkha-Nepal earthquake, *Geophys. J. Int.*, *203*, 2119–2124, doi:10.0193/gji/ggv412.
- Avouac, J.-P. (2003), Mountain building, erosion and the seismic cycle in the Nepal Himalaya, *Adv. Geophys.*, *46*, 1–80.
- Avouac, J.-P., L. Meng, S. Wei, T. Wang, and J.-P. Ampuero (2015), Lower edge of locked Main Himalayan Thrust unzipped by the 2015 Gorkha earthquake, Nepal, *Nature*, *8*, 708–711, doi:10.1038/NGEO2518.
- Berger, A., F. Jouanne, R. Hassani, and J. L. Mugnier (2004), Modelling the spatial distribution of present-day deformation in Nepal: How cylindrical is the Main Himalayan Thrust in Nepal?, *Geophys. J. Int.*, *156*, 94–114, doi:10.1111/j.1365-246X.2004.02038.x.
- Bettinelli, P., J.-P. Avouac, M. Flouzat, F. Jouanne, L. Bollinger, P. Wills, and G. R. Chitrakar (2006), Plate motion of India and interseismic strain in the Nepal Himalaya from GPS and DORIS measurements, *J. Geod.*, *80*, 567–589, doi:10.1007/s00190-006-0030-3.
- Bilham, R. (2015), Raising Kathmandu, *Nat. Geosci.*, *8*, 582–584.
- Bilham, R., V. K. Gaur, and P. Molnar (2001), Himalayan seismic hazard, *Science*, *293*, 1442–1444.
- Cattin, R., and J.-P. Avouac (2000), Modeling mountain building and the seismic cycle in the Himalaya of Nepal, *J. Geophys. Res.*, *105*, 13,389–13,407, doi:10.1029/2000JB900032.
- Chuang, R. Y., K. M. Johnson, Y.-M. Wu, K. E. Ching, and L. C. Kuo (2013), A midcrustal ramp-fault structure beneath the Taiwan tectonic wedge illuminated by the 2013 Nantou earthquake series, *Geophys. Res. Lett.*, *40*, 5080–5084, doi:10.1002/grl.51005.
- Denolle, A. A., W. Fan, and P. M. Shearer (2015), Dynamics of the 2015 M 7.8 Nepal earthquake, *Geophys. Res. Lett.*, *42*, 7467–7475, doi:10.1002/2015GL065336.
- Diao, F., T. R. Walter, M. Motagh, P. Prats-Iraola, R. Wang, and S. V. Samsonov (2015), The 2015 Gorkha earthquake investigated from radar satellites: Slip and stress modeling along the MHT, *Front. Earth Sci.*, doi:10.3389/feart.2015.00065.
- Fan, W., and P. M. Shearer (2015), Detailed rupture imaging of the 25 April 2015 Nepal earthquake using teleseismic P waves, *Geophys. Res. Lett.*, *42*, 5744–5752, doi:10.1002/2015GL064587.
- Feldl, N., and R. Bilham (2006), Great Himalayan earthquakes and the Tibetan Plateau, *Nature*, *444*, 165–170, doi:10.1038/nature05199.
- Feng, G., Z. Li, X. Shan, L. Zhang, G. Zhang, and J. Zhu (2015), Geodetic model of the 2015 April 25 M_w 7.8 Gorkha Nepal earthquake and M_w 7.3 aftershock estimated from InSAR and GPS data, *Geophys. J. Int.*, *203*, 896–900, doi:10.1093/gji/ggv335.
- Feng, W., Z. Li, T. Hoey, Y. Zhang, R. Wang, S. Samsonov, Y. Li, and Z. Xu (2014), Patterns and mechanisms of coseismic and postseismic slips of the 2011 M_w 7.1 Van (Turkey) earthquake revealed by multi-platform synthetic aperture radar interferometry, *Tectonophysics*, *632*, 188–198, doi:10.1016/j.tecto.2014.06.011.
- Fialko, Y. (2004), Probing the mechanical properties of seismically active crust with space geodesy: Study of the co-seismic deformation due to the 1992 M_w 7.3 Landers (southern California) earthquake, *J. Geophys. Res.*, *109*, B01303, doi:10.1029/2003JB002756.
- Galetzka, J., et al. (2015), Slip pulse and resonance of Kathmandu basin during the 2015 M_w 7.8 Gorkha earthquake, Nepal imaged with geodesy, *Science*, *349*(6252), 1091–1095, doi:10.1126/science.aac6383.
- Global Centroid Moment Tensor Catalogue (GCMT) (2015). [Available at <http://www.globalcmt.org/CMTsearch.html>].
- Grandin, R., M. Vallee, C. Satriano, R. Lacassin, Y. Klinger, M. Simoes, and L. Bollinger (2015), Rupture process of the $M_w = 7.9$ 2015 Gorkha earthquake (Nepal): Insights into Himalayan megathrust segmentation, *Geophys. Res. Lett.*, *42*, 8373–8382, doi:10.1002/2015GL066044.
- Hsu, Y.-J., N. Bechor, P. Segall, S.-B. Yu, L.-C. Kuo, and K.-F. Ma (2002), Rapid afterslip following the 1999 Chi-Chi, Taiwan earthquake, *Geophys. Res. Lett.*, *29*(16), 1754, doi:10.1029/2002GL014967.
- Hutton, W., C. DeMets, O. Sanchez, G. Suarez, and J. Stock (2001), Slip kinematics and dynamics during and after the 1995 October 9 $M_w = 8.0$ Colima-Jalisco earthquake, Mexico, from GPS geodetic constraints, *Geophys. J. Int.*, *146*(3), 637–658, doi:10.1046/j.1365-246X.2001.00472.x.
- Jouanne, F., J. Mugnier, J. Gamond, P. Le Fort, M. Pandey, L. Bollinger, M. Flouzat, and J.-P. Avouac (2004), Current shortening across the Himalayas of Nepal, *Geophys. J. Int.*, *157*, 1–14, doi:10.1002/2014JB010970.
- Jouanne, F., A. Awan, A. Madji, A. Pécher, M. Latif, A. Kausar, J. L. Mugnier, I. Khan, and N. A. Khan (2011), Postseismic deformation in Pakistan after the 8 October 2005 earthquake: Evidence of afterslip along a flat north of the Balakot-Bagh thrust, *J. Geophys. Res.*, *116*, B07401, doi:10.1029/2010JB007903.
- Lemonnier, C., G. Marquis, F. Perrier, J.-P. Avouac, G. Chitrakar, B. Kafle, S. Sapkota, U. Gautam, D. Tiwari, and M. Bano (1999), Electrical structure of the Himalaya of Central Nepal: High conductivity around the mid-crustal ramp along the MHT, *Geophys. Res. Lett.*, *26*, 3261–3264, doi:10.1029/1999GL008363.

- Lindsey, E., R. Natsuaki, X. Xu, M. Shimada, H. Hashimoto, D. Melgar, and D. Sandwell (2015), Line of sight deformation from ALOS-2 interferometry: M_w 7.8 Gorkha earthquake and M_w 7.3 aftershock, *Geophys. Res. Lett.*, *42*, 6655–6661, doi:10.1002/2015GL065385.
- Marone, C. J., C. H. Scholz, and R. Bilham (1991), On the mechanics of earthquake afterslip, *J. Geophys. Res.*, *96*, 8441–8452, doi:10.1029/91JB00275.
- Mugnier, J.-L., A. Gajurel, P. Huyghe, R. Jayagondaperumal, F. Jouanne, and B. Upreti (2013), Structural interpretation of the great earthquakes of the millennium in the central Himalaya, *Earth Sci. Rev.*, *127*, 30–47.
- Okada, Y. (1985), Surface deformation due to shear and tensile faults in a half-space, *Bull. Seismol. Soc. Am.*, *75*(4), 1135–1154.
- Pandey, M., R. Tankadar, J.-P. Avouac, J. Lavé, and J.-P. Massot (1995), Interseismic strain accumulation on the Himalayan crustal ramp (Nepal), *Geophys. Res. Lett.*, *22*, 751–754, doi:10.1029/94GL02971.
- Parameswaran, R. M., T. Natarajan, K. Rajendran, C. P. Rajendran, R. Mallick, M. Wood, and H. C. Lekhak (2015), Seismotectonics of the April–May 2015 Nepal earthquakes: An assessment based on the aftershock patterns, surface effects and deformational characteristics, *J. Asian. Earth. Sci.*, *111*, 161–174, doi:10.1016/j.jseae.2015.07.030.
- Sapkota, S. N., L. Bollinger, Y. Klinger, P. Tapponnier, Y. Gaudemer, and D. Tiwari (2012), Primary surface ruptures of the great Himalayan earthquakes in 1934 and 1255, *Nat. Geosci.*, *6*, 71–76, doi:10.1038/ngeo1669.
- Satyabala, S. P., and R. Bilham (2006), Surface deformation and subsurface slip of the 28 March 1999 $M_w = 6.4$ west Himalayan Chamoli earthquake from InSAR analysis, *Geophys. Res. Lett.*, *33*, L23305, doi:10.1029/2006GL027422.
- Scholz, C. H. (1990), *The Mechanics of Earthquakes and Faulting*, Cambridge Univ. Press, Cambridge, U. K.
- U.S. Geological Survey–National Earthquake Information Center (USGS–NEIC) (2015). [Available at <http://earthquake.usgs.gov/earthquakes/search/>.]
- Wang, K., and Y. Fialko (2015), Slip model of the 2015 M_w 7.8 Gorkha (Nepal) earthquake from inversion of ALOS-2 and GPS data, *Geophys. Res. Lett.*, *42*, 7452–7458, doi:10.1002/2015GL065201.
- Wang, R. J., S. Parolai, M. R. Ge, M. P. Jin, T. R. Walter, and J. Zschau (2013), The 2011 M_w 9.0 Tohoku earthquake: Comparison of GPS and strong-motion data, *Bull. Seismol. Soc. Am.*, *103*, 1336–1347, doi:10.1785/0120110264.
- Wobus, G., A. Heimsath, K. Whipple, and K. Hodges (2005), Active out-of-sequence thrust faulting in the central Nepalese Himalaya, *Nature*, *434*, 1008–1011.
- Yagi, Y., and R. Okuwaki (2015), Integrated seismic source model of the 2015 Gorkha, Nepal earthquake, *Geophys. Res. Lett.*, *42*, 6229–6235, doi:10.1002/2015GL064995.
- Zhang, G., E. Hetland, and X. Shan (2015), Slip in the 2015 M_w 7.9 Gorkha and M_w 7.3 Kodari, Nepal, earthquakes revealed by seismic and geodetic data: Delayed slip in the Gorkha and slip deficit between the two earthquakes, *Seismol. Res. Lett.*, *86*(6), 1578–1586, doi:10.1785/0220150139.
- Zhao, W., K. D. Nelson, J. Che, J. Quo, D. Lu, C. Wu, and X. Liu (1993), Deep seismic-reflection evidence continental underthrusting beneath southern Tibet, *Nature*, *366*, 557–559, doi:10.1038/366557a0.